A Pulse EPR and ENDOR Investigation of the Electronic Structure of a σ-Carbon-Bonded Cobalt(IV) Corrole

Jeffrey Harmer, Sabine Van Doorslaer, Igor Gromov, Martin Bröring,† Gunnar Jeschke,‡ and Arthur Schweiger*

Physical Chemistry, ETH Zurich, CH-8093 Zurich, Switzerland, Universität Würzburg, Institut für Anorganische Chemie, Am Hubland, D-97074 Würzburg, Germany, and Max-Planck-Institut für Polymerforschung, Postfach 3148, D-55021, Mainz, Germany

Received: August 24, 2001; In Final Form: November 26, 2001

In this contribution we present a continuous wave (CW), pulse electron paramagnetic resonance (EPR), and pulse electron nuclear double resonance (ENDOR) study of (OEC)Co(C_6H_5), where OEC is the trianion of 2,3,7,8,12,13,17,18-octaethylcorrole. To facilitate spectral assignments isotopic substitutions were employed (^{2}H and ^{13}C). From the analysis of the frozen solution CW EPR, ESEEM, and ENDOR spectra measured at X- and Q-band, we determined the electronic coupling parameters of the unpaired electron with the cobalt nucleus, corrole nitrogen nuclei, phenyl ^{13}C, ^{1}H and ^{2}H nuclei, meso ^{1}H and ^{2}H nuclei, and ethyl ^{1}H nuclei. Determination of the **g** matrix alignment in the molecular frame was achieved by successfully simulating the orientationally selective powder ENDOR spectra of the meso nuclei. The *g* principal values are $g_1 = 1.9670$, $g_2 = 2.1122$, and g_3=2.0043, with the $\mathbf{g}_1$ and $\mathbf{g}_2$ axes pointing at the nitrogens of the corrole macrocycle and the $\mathbf{g}_3$ axis directed perpendicular to the plane. The cobalt hyperfine matrix **A** has principal values $A_1^{Co} = 72$, $A_2^{Co} = 8$, $A_3^{Co} = 10$ MHz, with the $\mathbf{A}_3^{Co}$ and $\mathbf{g}_3$ axes parallel to each other and the $\mathbf{A}_1^{Co}$ axis rotated from the $\mathbf{g}_1$ axis by 45°, so that it points at the meso proton H10. Relatively large ^{1}H ENDOR couplings with the ethyl protons were observed, indicating that significant spin density also exists on the macrocycle. A good description of the electronic structure, consistent with the experimental data, was achieved using density functional theory simulations. Both the experimental and calculated data support the conclusion that there is significant spin density on both the macrocycle and in the cobalt d_{yz} orbital.

Introduction

The electronic structure of σ-carbon-bonded cobalt corrole complexes is of interest because of its relevance to the biochemistry of B_{12} coenzymes that are distinguished by a cobalt−carbon bond.[1,2] This has prompted the synthesis and chemical characterization of a variety of alkyl and aryl σ-bonded organocobalt complexes.[3] Electrochemically generated σ-carbon-bonded cobalt(III) porphyrin π cation radicals have been studied, but cobalt(IV) porphyrins have not yet been characterized.[4] However, a number of electrochemically generated Co(IV) and Co(II) metal complexes and Co(III) π cation radicals with a corrole macrocycle have been described.[5−7] The corroles are structurally similar to the porphyrins but have a smaller macrocycle core and differ in the charge of the deprotonated macrocycle, which is −3 for the corrole and −2 for the porphyrin. As a consequence, the corrole macrocycle is able to stabilize metal ions in higher oxidation states than the corresponding porphyrin macrocycle. Additionally, corroles are easier to oxidize than metalloporphyrins containing the same metal ion. Electrochemical studies of corroles containing the metal centers Co, Fe, Sn, Mn, Ni, Cu, Ti, As, Sb, and Bi have been reported, with cases being found where oxidation involves the metal center and others the conjugated macrocycle.[5,6,8−12]

In this study we investigate the complex (OEC)Co^{IV}(C_6H_5), where OEC is the trianion of 2,3,7,8,12,13,17,18-octaethylcorrole (Figure 1). The compound is a rare example of a stable five-coordinated σ-carbon-bonded cobalt complex in a high (+IV) oxidation state. Will et al.[7] studied the (OEC)Co(C_6H_5) complex using NMR and EPR spectroscopy, X-ray diffraction, electrochemistry, and magnetic susceptibility measurements. However, their results in terms of the electronic structure were only preliminary, particularly with respect to the EPR measurements where only *g* values from X-band continuous wave (CW) EPR measurements were reported. Two extreme formulations are possible to describe the distribution of the unpaired electron density. The unpaired electron can be localized on the cobalt ion and thus the complex formulated as a cobalt(IV) corrole, (OEC)Co^{IV}(C_6H_5), or the unpaired electron can be distributed over the macrocycle and thus formulated as a cobalt(III) corrole π radical, ($OEC^{\bullet+}$)Co^{III}(C_6H_5). Will et al.[7] proposed that the complex can be represented as a resonance hybrid between these two extremes, with the unpaired electron in the $d_{x^2-y^2}$ orbital of the cobalt ion, see Figure 1 (we use the corrole coordinate system, see note 13). The anisotropy of the principal *g* values ($g_1 = 2.12$, $g_2 = 2.01$, and $g_3 = 1.94$) observed in a frozen solution of CH_2Cl_2 supported the formation of a Co(IV) complex. In contrast, the ^{1}H NMR data showed ethyl resonances that were strongly broadened and shifted downfield, suggesting significant delocalization of the unpaired electron over the system of the corrole macrocycle and thus giving π cation radical character to the complex. Additionally, by comparing data obtained on samples where the phenyl ring had protons and then deuterons, small chemical shifts could be assigned to

* To whom correspondence should be addressed. E-mail: schweiger@esr.phys.chem.ethz.ch.
† Universität Würzburg.
‡ Max-Planck-Institut für Polymerforschung.

10.1021/jp013269t CCC: $22.00
Published on Web 02/16/2002

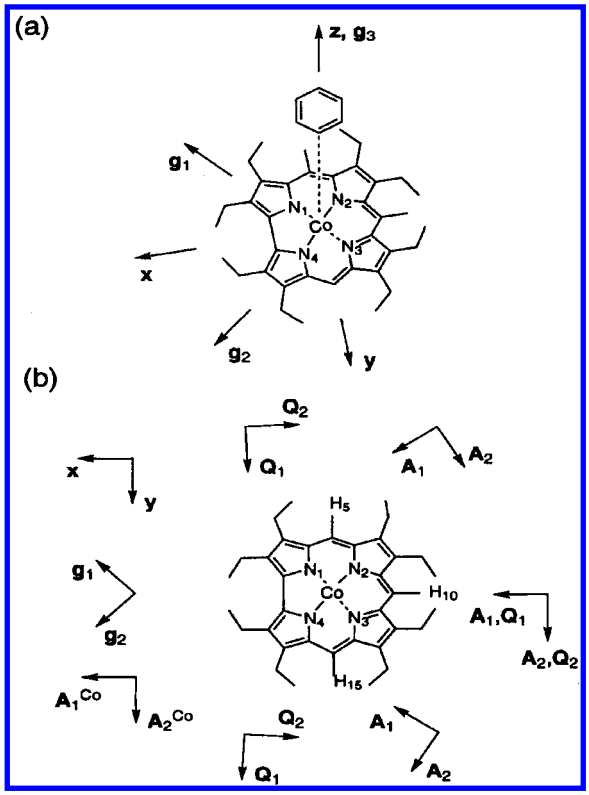

Figure 1. (a) Structure of (OEC)Co(C_6H_5) and orientation of the **g** principal axes and *x*, *y*, and *z* axes used to define the cobalt d orbitals. (b) Cobalt hyperfine ($\mathbf{A}^{Co}$) and meso nuclei hyperfine (**A**) matrixes and nuclear quadrupole tensors (**Q**) with principal axes in the plane of the macrocycle.[13]

the phenyl protons. Magnetic susceptibility measurements on crystals of (OEC)Co(C_6H_5), which exhibit a $\pi-\pi$ dimer structure as revealed by X-ray data analysis, were interpreted in favor of a complex with π cation radical character. However, it was not clearly stated how these data can be applied to the monomeric form of the complex present in frozen solution.

One- and two-dimensional pulse EPR and electron nuclear double resonance (ENDOR) techniques[14,15] allow paramagnetic compounds to be characterized in much greater detail than with classical CW EPR spectroscopy. In particular, the interactions of weakly coupled magnetic ligand nuclei, not resolved in the CW EPR spectrum, are often observed with these techniques. For (OEC)Co(C_6H_5), three-pulse electron spin−echo envelope modulation (ESEEM) and hyperfine sublevel correlation (HYSCORE) techniques proved to be ideal tools for measuring the hyperfine and nuclear quadrupole couplings of the ^{14}N corrole nuclei, and pulse ENDOR proved to be well suited to determine the interactions with the meso (^{1}H, ^{2}H), ethyl (^{1}H), and phenyl (^{1}H, ^{2}H, and ^{13}C) nuclei. The experimental results are supported and complemented by density functional calculations of the spin density distribution.

Materials and Methods

Sample Preparation. (σ-Phenyl)(2,3,7,8,12,13,17,18-octaethylcorrole)cobalt, (OEC)Co(C_6H_5), was prepared as described in ref 7, and complexes with deuterated phenyl protons (OEC)-Co(C_6D_5) and ^{13}C phenyl carbons (OEC)Co($^{13}C_6H_5$) were prepared using C_6D_5Br (99.5%) and $^{13}C_6H_5Br$ (99%), respectively (from Campro Scientific). The preparation of 5,10,15-trideutero-2,3,7,8,12,13,17,18-octaethylcorrole, (D_3−OEC)Co-(C_6H_5), started from the nondeuterated corrole as follows. 2,3,7,8,12,13,17,18-Octaethylcorrole (523 mg, 1 mmol) is dissolved in trifluoroacetic acid-*d* (5 mL, Aldrich, used as received) and stirred at room temperature for 30 min. After evaporation of all volatiles in vacuo, this process is repeated. The resulting solids are stirred with deuterium oxide before being dissolved in dichloromethane. The mixture is then neutralized with a solution of dry potassium carbonate in deuterium oxide; the organic layer was washed three times with deuterium oxide and dried with sodium sulfate. After evaporation of the solvent, the remaining product is recrystallized from methanol/chloroform to yield 501 mg (95%) of the title compound. As judged by NMR, the degree of deuteration in the *meso* positions is about 96−97%. Mass spectra (EI, 70 eV): *m*/*z* (%) 525 (100) M^+.

Samples for the EPR experiments were prepared in a glovebox with various solvents to a concentration of approximately 1 mM, transferred to an EPR tube and any remaining oxygen was removed by degassing on a vacuum line using the usual freeze−pump−thaw method. The solvents used were dichloromethane (CH_2Cl_2), toluene, methanol, tetrahydrofuran (thf), 2-methyl-tetrahydrofuran (mthf), acetone, and methanol (all from Fluka, puriss., over molecular sieves); chloroform ($CHCl_3$) (Fluka, for UV-spectroscopy), deuterium oxide (99.996%), and toluene-d_8 (99.6%) (Cambridge isotope laboratories, Inc.). Liquid crystals E7 and MLC-6204-00 were acquired from Merck.

Samples using a liquid crystal (LC) solvent were prepared by first dissolving (OEC)Co(C_6H_5) in toluene, mixing this solution with the LC, transferring it to an EPR tube and then removing the toluene on a vacuum line. Alignment of the LC was achieved by putting the EPR tube into the microwave cavity (in the nematic temperature range) with an external magnetic field of 1.2 T. After 10 min the sample was very rapidly cooled to 77 K by filling the dewar within the microwave (mw) cavity with liquid nitrogen. Measurements were performed at this initial orientation ($\theta = 0°$) and after a 90° rotation of the sample about the tube axis perpendicular to the external magnetic field ($\theta = 90°$). With slow cooling only a poor alignment of the complex in the LC was achieved.

Equipment. The X-band CW EPR spectra were measured on a Bruker ESP300 spectrometer (microwave (mw) frequency 9.45 GHz), equipped with a liquid nitrogen cyrostat. An mw power of 20 mW, a modulation amplitude of 0.1 mT, and a modulation frequency of 100 kHz were used. The Q-band CW EPR spectra were measured on a home-built instrument (mw frequency 35.3 GHz),[16] equipped with a liquid Helium cryostat from Oxford, Inc. An mw power of 20 mW, a modulation amplitude of 0.4 mT, and a modulation frequency of 100 kHz were used. The magnetic field at both X- and Q-band was measured with a Bruker NMR ER 035M gaussmeter.

The ESEEM and HYSCORE spectra were recorded at X-band using a Bruker Elexsys E580 spectrometer (mw frequency 9.73 MHz) equipped with a liquid Helium cryostat from Oxford, Inc. Measurements were done in frozen solutions of toluene at a temperature of 15 K and a repetition rate of 500 Hz. The following sequences were used:

Three-Pulse ESEEM.[15,17,18] Experiments were carried out using the pulse sequence $\pi/2$-τ-$\pi/2$-T-$\pi/2$-τ-echo with mw pulses of length $t_{\pi/2} = 24$ ns, a starting time $T_o = 96$ ns, and a time increment $\Delta T = 16$ ns (512 intervals). To remove blind spots, time τ was incremented from 96 to 1104 ns in steps of $\Delta\tau = 16$ ns.

HYSCORE.[15,19] Experiments were carried out using the pulse sequence $\pi/2$-τ-$\pi/2$-t_1-π-t_2-$\pi/2$-τ-echo with mw pulses of length $t_{\pi/2} = 24$ ns and $t_\pi = 16$ ns, a starting time of 96 ns for t_1 and

t_2, and a time increment $\Delta t = 16$ ns (data matrix 512 × 512); an eight-step phase cycle was used. Blind spots were checked for by comparing the spectra measured with τ values of 96, 196, and 296 ns.

The pulse ENDOR spectra were measured at Q-band at an mw frequency of 35.3 GHz.[16] The measurements were done in frozen solutions of toluene between 8 and 15 K at a repetition rate of 100 Hz using the following sequences.

Davies-ENDOR.[15,20] Experiments were carried out using the pulse sequence π-T-$\pi/2$-τ-π-τ-echo with a selective radio frequency (rf) π pulse of variable frequency applied during the time interval T. To detect ^{1}H (^{13}C) nuclei, an rf pulse of length 10 μs (50 μs) was applied. The mw pulse lengths were t_π = 200 ns, $t_{\pi/2}$ = 100 ns, and a τ value of 150 ns was used.

Mims-ENDOR.[15,21] Experiments were carried out using the pulse sequence $\pi/2$-τ-$\pi/2$-T-$\pi/2$-τ-echo with a selective rf π pulse of variable frequency applied during the time interval T. To observe ^{2}H (^{13}C) nuclei the rf pulse length was 75 μs (50 μs), the mw pulse length was $t_{\pi/2}$ = 24 ns, and time τ was 400 ns (150 ns). For the small ^{2}H couplings measured in these experiments, τ = 400 ns was optimal for maximum signal intensity and short enough to avoid blind spots,[22] which occur at $a = n/\tau$, where a is the hyperfine coupling and n is a positive integer (maximum sensitivity when $a\tau \sim 0.7$).

Data Manipulation. Data processing was done with MATLAB (The MathWorks, Inc.). The ESEEM and HYSCORE time traces were baseline corrected using a second-order polynomial, apodized with a Hamming window, and zero filled. After Fourier transformation the absolute-value spectra were calculated. To remove blind spots and deadtime dependent distortions in the three-pulse ESEEM data, spectra measured at different τ values were added.

Evaluation of the Spin Hamiltonian Parameters

The spin Hamiltonian for a paramagnetic species with a Co^{IV} ion (electronic configuration $3d^5$, $S = 1/2$, $I = 7/2$) and surrounding nuclei in frequency units is given by

$$\mathscr{H} = (\beta_e/h)\mathbf{B_o g S} + \mathbf{S A}^{Co}\mathbf{I} + \mathscr{H}_{nucl} \qquad (1)$$

The first term is the electron Zeeman interaction, the second term describes the hyperfine interaction between the unpaired electron and the nuclear spin of cobalt. The CW EPR spectrum of (OEC)Co(C_6H_5) is dominated by these two terms. $\mathscr{H}_{nucl}$ describes the interactions with the surrounding nuclei, which can be observed with ESEEM and ENDOR. For (OEC)Co(C_6H_5) these interactions arise from ^{14}N ($I = 1$), ^{13}C ($I = 1/2$), ^{1}H ($I = 1/2$), and ^{2}H ($I = 1$) nuclei. The spin Hamiltonian of an $S = 1/2$, $I = 1/2$ subsystem can be described in terms of the **g** matrix and the hyperfine matrix **A**. For weakly coupled nuclei ($|a| < 2\nu_I$), the ENDOR spectrum at a particular observer position consists of peaks at the two frequencies $\nu_{\alpha,\beta} = \nu_I \pm a/2$, centered at the nuclear Larmor frequency $\nu_I = g_n\beta_n B_o/h$ and split by the hyperfine interaction a. The hyperfine interaction can be split into an isotropic contribution a_{iso} determined by the spin density at the nucleus and an anisotropic contribution. By assuming a point−dipole interaction between the unpaired electron and the nucleus, the anisotropic contribution can be estimated by ref 15

$$T = (\mu_o/4\pi)(g g_n \beta_e \beta_n/hr^3) \qquad (2)$$

where r is the distance between the electron spin and the nucleus. The anisotropic part of the hyperfine matrix is described by the principal values $-T$, $-T$, and $2T$.

The spin Hamiltonian of an $S = 1/2$, $I = 1$ subsystem can be described in terms of the **g** matrix, the hyperfine matrix **A**, and the nuclear quadrupole tensor **Q**. This Hamiltonian gives rise to three nuclear transitions (two single-quantum (sq) transitions with $|\Delta m_I| = 1$ and one double-quantum (dq) transition with $|\Delta m_I| = 2$) between the nuclear sublevels in each electron spin manifold (α,β). The **Q** tensor is traceless and the principal values are usually expressed by the quadrupole coupling constant $K = e^2qQ/4h$, and the asymmetry parameter $\eta = (Q_x - Q_y)/Q_z$, with $Q_x = -K(1 - \eta)$, $Q_y = -K(1 + \eta)$, and $Q_z = 2K$.

In the ^{2}H ENDOR spectra recorded for (OEC)Co(C_6H_5), the $\nu_{\alpha,\beta}$ peaks are split by the quadrupole interaction with maximum splitting given by $6K$.[23] In our data only the $|\Delta m_I| = 1$ transitions are observed, as is usually the case.

In the ^{14}N ESEEM spectra all three nuclear frequencies within each nuclear spin manifold were observed, and in the HYSCORE spectra cross-peaks were observed between the three nuclear frequencies of the α and β manifolds.[24] Generally, the double-quantum transitions in the α and β manifolds give rise to sharp peaks in the spectrum, and their position may be estimated using the expression[25,26]

$$\nu_{dq\alpha,dq\beta} = 2[(\nu_I \pm a/2)^2 + K^2(3 + \eta^2)]^{1/2} \qquad (3)$$

The single-quantum cross-peaks in both nuclear spin manifolds are usually distinguished by significant anisotropic line broadening and are often not observed. In the "exact cancellation" case where $|a| \approx 2\nu_I$, the effective field experienced by the nucleus in one of the two nuclear spin manifolds vanishes. Three low-frequency lines are then observed in ESEEM spectra which provide initial guesses for the nuclear quadrupole parameters using

$$\nu_o = 2K\eta, \quad \nu_- = K(3 - \eta), \quad \nu_+ = K(3 + \eta) \qquad (4)$$

where ν_o, ν_-, and ν_+ are the nuclear quadrupole frequencies. The double-quantum frequency ν_{dq} in the other manifold, where the local hyperfine field at the nucleus adds to the applied magnetic field, allows an estimation of the hyperfine parameters using eq 3. The ^{14}N corrole nuclei in (OEC)Co(C_6H_5) were ideally studied with ESEEM and HYSCORE since their magnetic parameters fulfill approximately the "exact cancellation" condition at X-band.

Simulation Procedures. Refined **g** and cobalt hyperfine matrixes were obtained from the experimental CW EPR spectra using the Bruker WinEPR program and the EasySpin program.[27] Simulation of the three-pulse ESEEM and HYSCORE spectra for disordered $S = 1/2$, $I = 1$ systems were achieved using programs written in-house.[28,29] For the ENDOR simulations the MAGRES program package was used.[30]

Density Functional Computations. Spin-unrestricted density functional computations of hyperfine and nuclear quadrupole couplings were performed with the Amsterdam Density Functional (ADF 2000.01)[31−34] and Gaussian 98 packages[35] on the basis of the published X-ray geometry of (OEC)Co(C_6H_5).[7] Only the heavy atom positions were used: protons were attached in Titan[36] on the basis of the Merck molecular force field.[37−39] For comparison, a geometry optimization for Co(corrin)(C_6H_5), i.e., without the eight ethyl substituents on the macrocycle, was performed with the BLYP density functional and a triple-ζ basis set with single polarization functions (basis set IV in ADF). For the computations of EPR parameters in ADF we used the BLYP functional and a triple-ζ basis set with single polarization

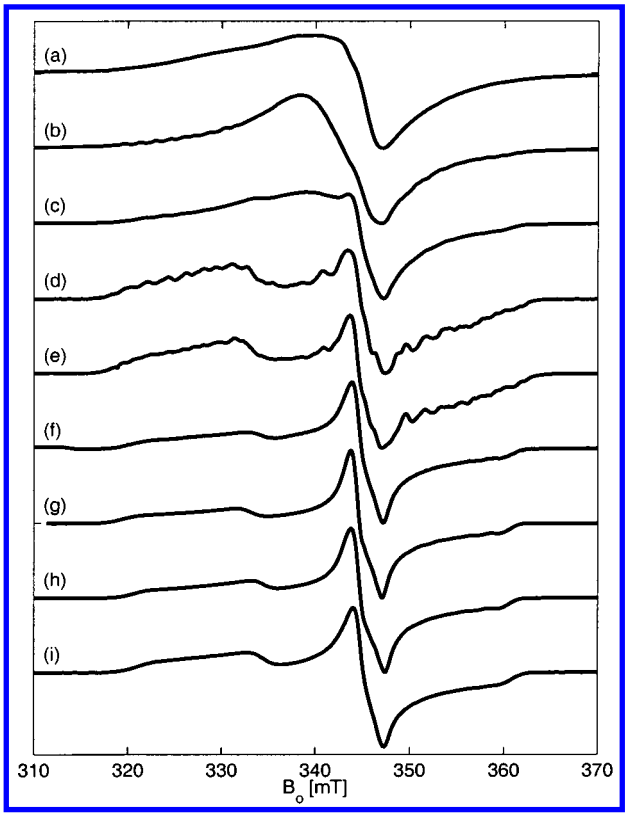

Figure 2. X-band CW EPR spectra measured at 120 K. (a) Polycrystalline (OEC)Co(C_6H_5). (b−i) (OEC)Co(C_6H_5) in CH_2Cl_2 (b), $CHCl_3$ (c), thf (d), acetone (e), methanol (f), mthf (g), toluene (h), and unorientated liquid crystal (i).

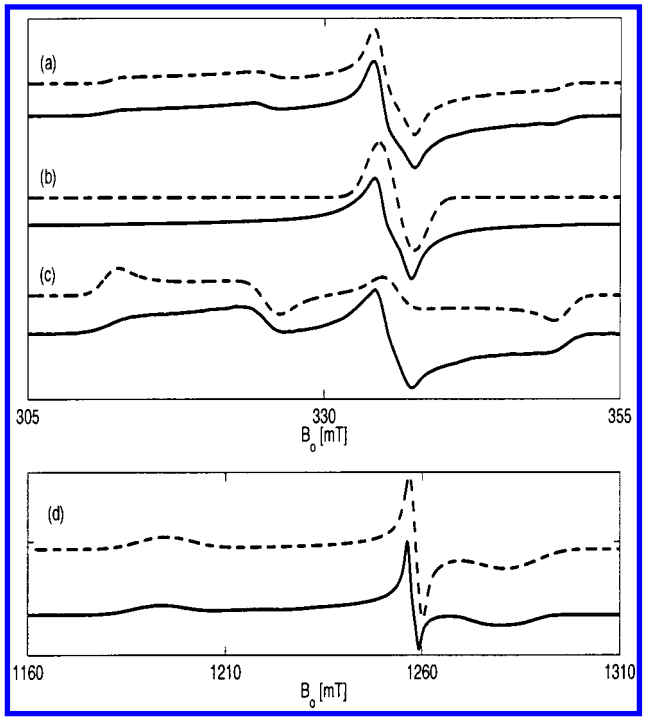

Figure 3. (a−c) Experimental (full lines) and simulated (dashed lines) X-band CW EPR spectra of (OEC)Co(C_6H_5) in a frozen toluene solution (120 K) (a), aligned in liquid crystal E7 at orientation θ=0° (b), and θ=90° (c). (d) Q-band CW EPR spectrum of (OEC)Co(C_6H_5) in a frozen toluene solution (120 K).

functions within the zeroth-order relativistic approximation (basis set ZORA IV).[40] The initial guess for the self-consistent field iteration was provided by the result of a single-point computation with a double-ζ basis set without polarization functions (ZORA II) to improve the convergence behavior with the larger basis set. Electron density cubes for the α and β spins and a density cube for the singly occupied molecular orbital (SOMO) were computed with 10 pm resolution using the auxiliary program DENSF within the ADF package. In the Gaussian 98 computations we used the B3LYP functional and the 6-31G* basis set. Nuclear quadrupole moments for the computation of the nuclear quadrupole tensors from the electric field gradient tensors were taken from ref 41. Data analysis and visualization were performed with a home-written program based on Matlab (The Math Works, Inc.).

Results

Solvent Interactions. Figure 2 shows the CW EPR spectra of polycrystalline (OEC)Co(C_6H_5) and of (OEC)Co(C_6H_5) in a variety of frozen solutions and in liquid crystal E7 (not orientated). The powder spectrum (Figure 2a) and the frozen solution spectra in CH_2Cl_2, $CHCl_3$, thf, and acetone (Figure 2b−e) are all slightly different and not reproducible. The EPR spectrum of (OEC)Co(C_6H_5) in CH_2Cl_2 was reported earlier.[7] The spectra in methanol, mthf, toluene, and the liquid crystal are very similar (Figure 2f−i). We also observed that the spectrum in $CHCl_3$ (Figure 2c) varied with concentrations from 10^{-2} to 10^{-5} M, with the spectrum at the lowest concentration being similar to that in toluene. No electron spin−echo signal at X-band was observed in a frozen solution of CH_2Cl_2 (at 10^{-3} M) and careful freezing of the sample was a prerequisite in all solvents to obtain reproducible CW EPR results. For example, sometimes crystallization of the toluene solvent resulted in partial alignment of the (OEC)Co(C_6H_5) molecules and therefore a distorted CW EPR spectrum, a phenomenon noted before for other complexes in toluene.[42]

The variations of the CW EPR spectra observed in Figure 2 are clearly caused by the poor glass-forming properties of some of the solvents. For example, in frozen solutions of CH_2Cl_2 the similarity of the CW EPR spectrum to that obtained from a concentrated powder and the lack of an electron spin−echo suggest that agglomeration of the (OEC)Co(C_6H_5) molecules occurs, resulting in strong electron−electron interactions and a distorted CW EPR spectrum. All further measurements in this work are thus made in frozen solutions of toluene, see Figure 2h.

g and A^{Co} Matrixes. The CW EPR spectra of (OEC)Co(C_6H_5) in toluene measured at 120 K at X- and Q-band are shown in Figure 3, along with the simulated spectra obtained using the parameters given in Table 1. The spectra are rhombic, with only partially resolved cobalt hyperfine couplings at X-band and no observable hyperfine structure at Q-band, indicating the existence of considerable **g** and **A** strain. The simulations were achieved with noncoaxial **g** and **A** principal axes directions, with the cobalt hyperfine matrix rotated by $\alpha_1 = 45°$ around the $\mathbf{g}_3$ axis (see Figure 1). The possibility of formation of (OEC)Co(C_6H_5) dimers in solution, which occurs in the solid state and also in solutions of related corrole complexes,[6,43] was excluded since no half-field signal could be observed. The cobalt hyperfine simulations were further supported by Q-band HYSCORE and ENDOR measurements at both X- and Q-band (see Figures 1S and 2S in Supporting Information).

We orientated the complex in the nematic phase of an LC to get additional information about the **g** principal axes directions.[44] Figure 3b−c shows the experimental and simulated spectra when

TABLE 1: Principal *g* Values and Metal Hyperfine Couplings *A* of (OEC)Co(C_6H_5) and Related Complexes, along with the d Orbital Contribution to the SOMO

complex	g_1	g_2	g_3	$\|A_1\|$ (MHz)	$\|A_2\|$ (MHz)	$\|A_3\|$ (MHz)	SOMO	ref
(OEC)$Co^{IV}(C_6H_5)$[a]	1.9670	2.1122	2.0043	72	8	10	d_{yz}	this work
(OEC$^{\bullet+}$)Ni^{II} at 298 K[b]	g = 2.01, ΔB = 4.5 mT at 298 K g = 2.011, 1.998 ΔB = 1.1 mT at 200 K						π cation radical	12
$[(OEC^{\bullet+})Co]_2^{+1,+2}$ [c]	g = 2.00 and ΔB = 4.5 mT at 77 K			no detectable hyperfine structure			π cation radical	6
$((OEC)Sn(C_6H_5))^{+\bullet}$ [d]	g = 2.00 and ΔB = 2.4 mT at 298 K g = 2.00 and ΔB = 5.0 mT at 130 K						π cation radical	10
$((OEC)Fe^{III}(C_6H_5))^-$ [e]	1.93	2.19	2.51					58
$((OEC)Fe(C_6H_5))^+$ [f]	2.01	2.04	2.17					58
$((OMTPC)Co^{IV}(PPh_3))^+$ [g]	2.14	2.00	1.89					5
$Co(S_2C_2(CF_3)_2)_2(P(OPh)_3)$	$g_{\|\|} \sim 1.99$ $g_\perp \sim 2.03$			$A_{\|\|} \sim 183$ $A_\perp \sim 21$			d_{yz}/d_{xz}	59
organobis(dioximato)Co^{IV} complexes	$g_{\|\|} \sim 2.016-2.037$ $g_\perp \sim 2.022-2.031$			$A_{\|\|} \sim 75-105$ $A_\perp \sim 12-17$			$d_{x^2-y^2}$	60
Co(II)(amben)	2.6589	1.9814	2.0068	10	88	72	d_{yz}	74
Co(II)(acacen)[h]	3.26	1.88	2.00	347	112	103	d_{yz}	74
Co(II)(CF_3acacen)	3.562	1.80	1.86	627	93	75	d_{yz}	74
(oxyCo)TPP(py)[i]	2.0020	1.9827	2.0705	53.0	21.4	22.7	d_{yz}	75
(oxyCo)TPP(1-MeIm)[i]	2.0029	1.9836	2.0729	52.5	21.5	22.5		

[a] The principal axes $\mathbf{A}_1^{Co}$ and $\mathbf{A}_2^{Co}$ are rotated by $\alpha_1 = 45°$ around the principal axis $\mathbf{g}_3$, so $\mathbf{A}_1^{Co}||\mathbf{x}$, $\mathbf{A}_2^{Co}||\mathbf{y}$ and $\mathbf{A}_3^{Co}||\mathbf{z}$ (see Figure 1). The line widths at X-band were 1.7, 0.9, 1.7 mT, and 10, 1.5, and 10 mT at Q-Band. [b] Example of a π cation radical. [c] Example of a π cation radical, generated in PhCN with addition of pyridine, Cl^- or imidazole. [d] Example of a π anion radical. [e] Example of a d^5 low-spin iron(III) complex. [f] Although being assigned as a π cation radical, this complex is formally described as a $S = {}^1/_2$ derivative due to strong antiferromagnetic coupling between the unpaired electron of the π corrole radical electron ($S_R = {}^1/_2$) and the electrons of the metal center ($S_M = 1$). [g] Example of an electrogenerated Co(IV) complex, (OMPC)Co(PPh_3) is (5,10,15-tri-phenyl-2,3,7,8,12,13,17,18-octamethylcorrolato)cobalt triphenylphosphine. [h] The principal axes **g** and **A** are rotated by 45° in the molecular plane. [i] The principal **g** and $\mathbf{A}^{Co}$ axes are not coaxial.

the LC is orientated along $\mathbf{B}_o$ in the mw resonator ($\theta = 0°$) and after rotation by $\theta = 90°$. The simulation for $\theta = 0°$ was calculated with the $\mathbf{g}_3$ axis directed along $\mathbf{B}_o$, and the simulation for $\theta = 90°$ by including all orientations in the plane spanned by the $\mathbf{g}_1$ and $\mathbf{g}_2$ axes. The remaining deviations of the simulations are most likely due to the limited ordering of the molecules in the LC.

There are two possible interpretations of the spectra. First, assume that the LC orientates (OEC)Co(C_6H_5) in a similar way as is found in flat porphyrin complexes without axial ligands.[45,46] In the porphyrins the plane of the macrocycle is aligned along the LC so that for the $\theta = 0°$ orientation all in-plane g values will be observed, and for the $\theta = 90°$ orientation the features of the direction perpendicular to the plane are enhanced. For (OEC)Co(C_6H_5) the $\mathbf{g}_3$ axis is selected for $\theta = 0°$, which implies that the g_3 principal value is one of the two principal values which lie in the plane of the macrocycle. The complex is thus aligned only along this direction and discrimination between the $\mathbf{g}_1$ and $\mathbf{g}_2$ principal axes directions is not possible. The other alternative is to assume that the plane of the macrocycle is orientated at 90° to the LC, implying that the $\mathbf{g}_3$ principal axis is perpendicular (observed for $\theta = 0°$) and the $\mathbf{g}_1$ and $\mathbf{g}_2$ axes are parallel to the plane of the macrocycle (enhanced for $\theta = 90°$). The corrole complex contains rather bulky ethyl groups and the phenyl ring, which could change the alignment from that found for the flat porphyrin complexes with no axial ligands. It was possible to distinguish between these two cases by using orientationally selective deuterium ENDOR data of the meso nuclei (see below).

Interactions with Surrounding Protons (and Deuterons)

The ^1H (^2H) interactions were measured using Davies-ENDOR (Mims-ENDOR) at Q-band at different magnetic field settings to provide orientational selectivity.[47] To facilitate identification of the different resonances (OEC)Co(C_6H_5), (D_3-OEC)Co(C_6H_5), and (OEC)Co(C_6D_5) were studied in protonated and deuterated toluene.

Figure 4a shows the ^1H ENDOR spectra at six field positions for (OEC)Co(C_6H_5) in deuterated toluene. Hyperfine couplings from the meso protons could be unambiguously resolved by subtracting the (D_3-OEC)Co(C_6H_5) spectra from the corresponding (OEC)Co(C_6H_5) spectra (in deuterated toluene), as shown in Figure 5. The difference signal in Figure 5 is mainly due to the meso protons and reveals a hyperfine coupling of $|a| \sim 2$ MHz at $B_0 = 1259.8$ mT. The ^2H Mims-ENDOR spectra of (D_3-OEC)Co(C_6H_5) in toluene measured at different field positions showed well-resolved hyperfine and nuclear quadrupole couplings (Figure 6a). The ^1H difference signal from Figure 5 is also plotted at the corresponding field position after scaling by the gyromagnetic ratios ($g_{n,^1H}/g_{n,^2H} = 6.514$), which allows the nuclear quadrupole splitting to be identified. Figure 6b shows the simulated spectra and Figure 1b shows the orientation of the **A** matrix and **Q** tensor principal axes. The hyperfine and nuclear quadrupole parameters for the three meso nuclei obtained from the simulations are collected in Table 2. For all three nuclei the $\mathbf{A}_3$ and $\mathbf{Q}_3$ axes directions are coaxial to the $\mathbf{g}_3$ axis, and $\mathbf{A}_1$ and $\mathbf{Q}_1$ are rotated from the $\mathbf{g}_1$ axis by the angles α_2 and α_3 respectively. The successful simulation of the ENDOR

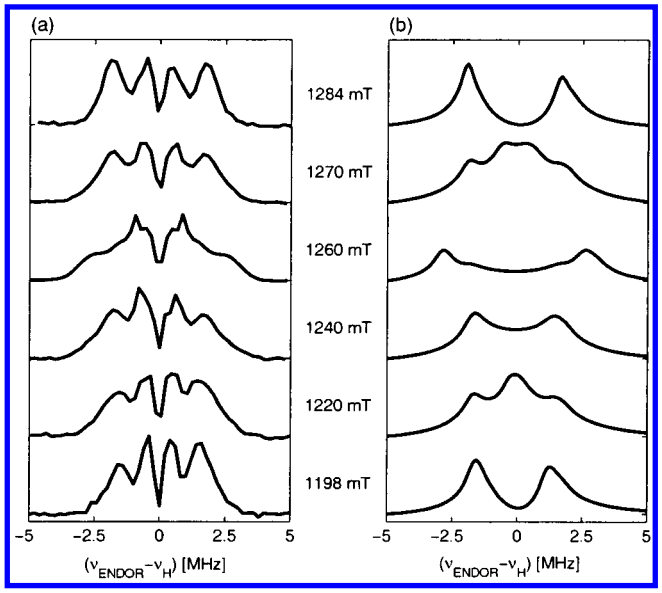

Figure 4. (a) Q-band ^{1}H Davies-ENDOR spectra of (OEC)Co(C_6H_5) in deuterated toluene at different observer fields. (b) Simulation of the largest proton couplings assigned to the ethyl protons.

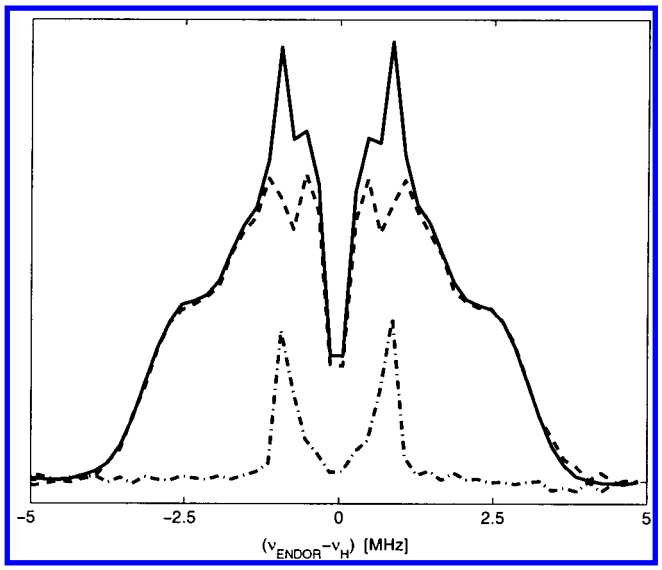

Figure 5. Q-band ^{1}H Davies-ENDOR spectra of (OEC)Co(C_6H_5) (full lines) and (D_3−OEC)Co(C_6H_5) (dashed lines) in deuterated toluene measured at B_0 = 1259.8 mT, together with the calculated difference spectrum (dashed−dotted lines).

spectra of the meso nuclei also allows determination of the **g** axes directions in the molecular frame by assuming that the largest value of the nuclear quadrupole tensor (Q_1) points along the H−C bond, as is generally observed.[48−52] Note that the angle between the H_5−C bond direction and the H_{10}−C (H_{15}−C) bond direction is 93° (187°), which is consistent with angle α_3 in Table 2. With this knowledge the nuclear quadrupole parameters infer that the $\mathbf{g}_3$ axis is normal to the corrole plane, with the $\mathbf{g}_1$ ($\mathbf{g}_2$) axis lying in the corrole plane and pointing toward the corrole nitrogen N_1 (N_4) (see Figure 1). The **A** matrix for the three meso protons is sensitive to the spin density distribution. For nucleus H_{10} the **A** matrix is coaxial to the **Q** tensor with $\mathbf{A}_1$ pointing along the C−H bond and consequently at the cobalt ion. For both H_5 and H_{15} the **A** matrix is not coaxial to the **Q** tensor, with the $\mathbf{A}_1$ direction of H_5 (H_{15}) pointing approximately at the nitrogen N_1 (N_4).

The phenyl ^{1}H and ^{2}H ENDOR signals are weak and difficult to detect. With Davies-ENDOR only small ^{1}H hyperfine

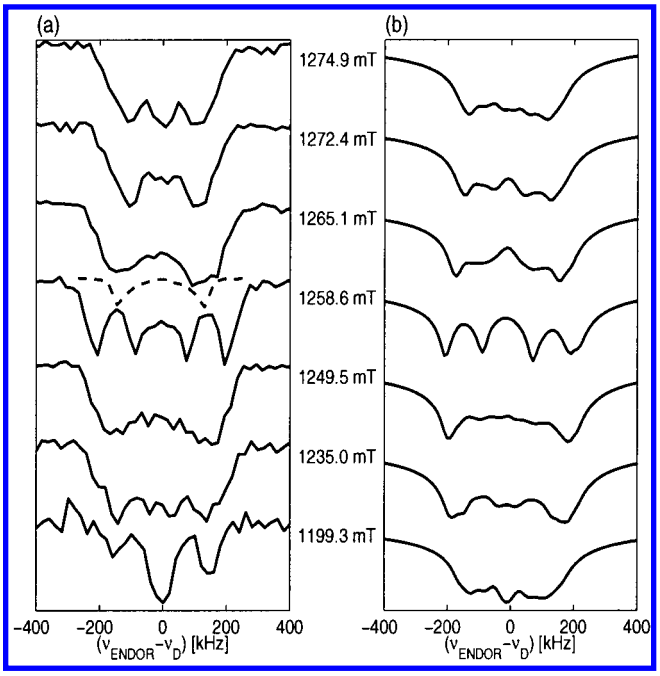

Figure 6. Q-band ^{2}H Mims-ENDOR spectra of the meso deuterium of (D_3−OEC)Co(C_6H_5) in toluene. (a) Measured spectra. The ^{1}H difference signal from Figure 5 is also shown (frequency axis scaled by 6.514). (b) Simulation of the spectra in (a).

couplings of $|a|<2$ MHz could be identified by subtracting the (OEC)Co(C_6D_5) spectra from the corresponding (OEC)Co(C_6H_5) spectra. Estimates from ^{2}H Mims-ENDOR spectra of (OEC)-Co(C_6D_5) were in agreement with the ^{1}H data. Therefore, the large and anisotropic couplings of approximately 3−6 MHz found in the ^{1}H ENDOR spectra of (OEC)Co(C_6H_5) (see Figure 4) cannot be assigned to either the meso or the phenyl protons. There are two possible sources of strong proton interactions, (a) coordination of a solvent molecule in an axial position, making the complex six coordinated or (b) interactions with the ethyl protons of the corrole macrocycle. The possibility of a sixth axial ligand was investigated experimentally by dissolving the complex in deuterated solvents, such as D_2O/toluene-d_8 mixtures, and then looking for a decrease in the ^{1}H ENDOR signal intensity of the unassigned coupling. The lack of any change in these ENDOR spectra confirmed that no direct coordination to the complex occurred. Therefore, we assign these couplings to interactions with the ethyl protons, as will be discussed further. Simulation for the ethyl proton(s) with the largest coupling(s) are shown in Figure 4b and the parameters are listed in Table 2.

Interaction with Phenyl Carbons

At both X- and Q-band ^{13}C ENDOR spectra of (OEC)Co-($^{13}C_6H_5$) in toluene were measured at a variety of field positions (see Figures 3S and 4S in Supporting Information). In Figure 7 we show a Q-band Davies- and Mims-ENDOR spectrum recorded at a field of B_o = 1270 mT. The largest splitting of ~4 MHz was found to be quasi-isotropic and was assigned to the directly coordinated ^{13}C nuclei of the phenyl ring (see Table 3). The smaller couplings (<0.75 MHz), werealso quasi-isotropic and belong to the meta, ortho, and para carbons.

Interaction with Corrole ^{14}N Nuclei

Interactions of the four ^{14}N nuclei of the corrole macrocycle were studied with three-pulse ESEEM and HYSCORE at

TABLE 2: Principal Values of Proton Hyperfine and Deuterium Nuclear Quadrupole Interactions

nucleus	A_1 (MHz)	A_2 (MHz)	A_3 (MHz)	α_2 (°)	Q_1 (kHz)	Q_2 (kHz)	Q_3 (kHz)	α_3 (deg)
meso 5[a]	−0.3	1.2	1.85	80	+102	−60	−42	138
meso 10[a]	0.7	1.3	1.85	47	+102	−60	−42	47
meso 15[a]	−0.3	1.2	1.85	10	+102	−60	−42	132
phenyl		< 2						
ethyl(s)	−3.7	−3.1	5.7					

[a] Both α_2 and α_3 define right-hand rotations of the $\mathbf{A}_1$ and $\mathbf{Q}_1$ axis (from $\mathbf{g}_1$) around the $\mathbf{g}_3$ axis, with $\mathbf{A}_3$ and $\mathbf{Q}_3$ parallel to the $\mathbf{g}_3$ axis (see Figure 1).

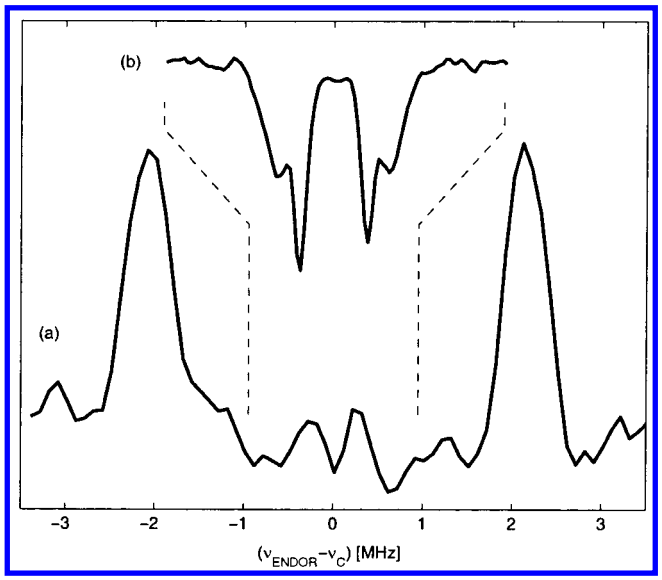

Figure 7. Q-band ENDOR spectra of (OEC)Co($^{13}C_6H_5$) in toluene at $B_o = 1270$ mT. (a) Davies-ENDOR for large hyperfine couplings. (b) Mims-ENDOR in the region $\nu_{13C} \pm 0.95$ MHz for small hyperfine couplings.

TABLE 3: Principal Values of Hyperfine Interactions for Phenyl ^{13}C Nuclei

nucleus	$\lvert A_1\rvert^b$ (MHz)	$\lvert A_2\rvert^b$ (MHz)	$\lvert A_3\rvert^b$ (MHz)
directly coordinated[a]	4.2	4.2	4.0

[a] Hyperfine matrix **A** is coaxial to the **g** matrix.

X-band. The three-pulse ESEEM spectra for three field positions are shown in Figure 8a and a HYSCORE spectrum measured at 342.0 mT is shown in Figure 9. The three-pulse ESEEM spectra consist of three prominent lines at approximately 0.4, 1.2 and 1.6 MHz which do not vary significantly with field position and satisfy the additivity relationship for a pure nuclear quadrupole interaction, i.e., $\nu_o + \nu_- = \nu_+$. The HYSCORE spectrum in Figure 9 shows strong cross-peaks between these three frequencies in one manifold and the double-quantum frequency in the other manifold as indicated in the figure. Examination of the three-pulse ESEEM and HYSCORE spectra at different field positions (not shown) revealed that the double-quantum peak varies between approximately 4.2−4.5 MHz. The other peaks in Figure 8a and Figure 9 belong to the two remaining single-quantum transitions and to combination peaks. It is evident that the ^{14}N nuclei are close to the exact cancellation condition, $|a| \sim 2\nu_N$ at all field positions and we can estimate the nuclear quadrupole and hyperfine frequencies using eqs 3 and 4, $\nu_o = 2K\eta \sim 0.42$ MHz, $\nu_- = K(3 - \eta) \sim 1.18$ MHz, and $\nu_+ = K(3 + \eta) \sim 1.60$ MHz yielding $K = 0.4633$ MHz and $\eta = 0.4464$ MHz. For $\nu_{dq} = 4.2-4.6$ MHz and using eq 3 with $\nu_N = 1.05$ MHz gives $|a| = 1.7-2.2$ MHz. Further refinement of the parameters was achieved by simulation. The parameters are listed in Table 4 and the simulated ESEEM spectra are show in Figure 8b. The $\mathbf{Q}_3$ axis is coaxial to the $\mathbf{g}_3$ axis, and the $\mathbf{Q}_1$ axis lies in the corrole plane and is at 90° to the Co−N bond (see Discussion). It was found that simulations using two equivalent ^{14}N nuclei was sufficient to obtain the general characteristics of the experimental spectra. Correspondence between experimental and simulated spectra could not be increased by considering the ^{14}N nuclei to be nonequivalent or including all four nuclei, due to the low resolution of the frozen solution measurements and the complexity of the spin system with four $I = 1$ nuclei.

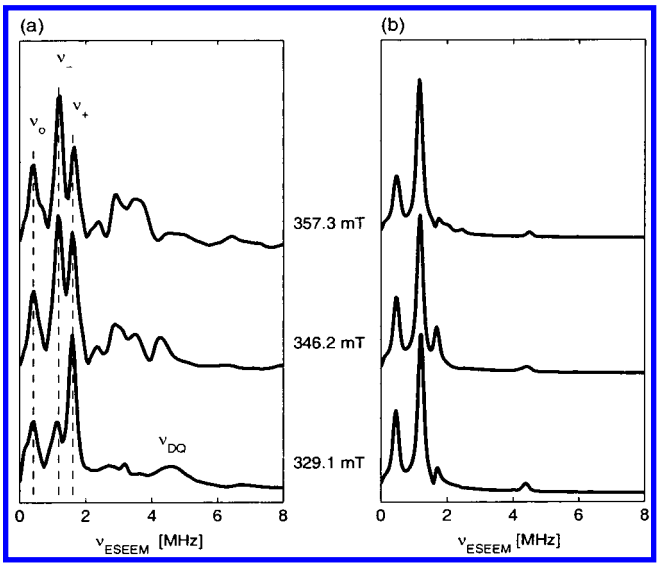

Figure 8. X-band three-pulse nitrogen ESEEM spectra of (OEC)Co(C_6H_5) measured in toluene at different observer positions. (a) Experimental. (b) Simulation.

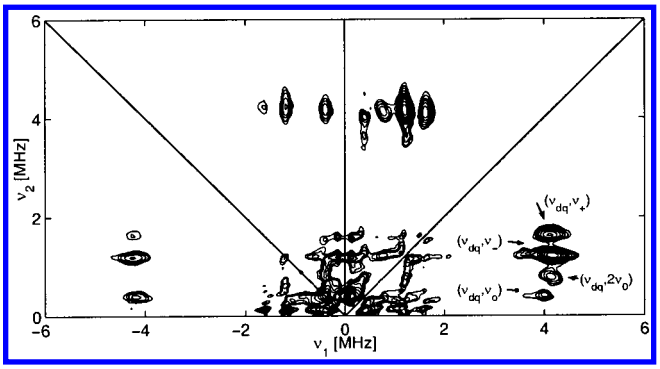

Figure 9. X-band nitrogen HYSCORE spectrum of (OEC)Co(C_6H_5) in toluene measured at $B_0 = 342.0$ mT.

TABLE 4: Principal Values of Hyperfine and Nuclear Quadrupole Interactions for ^{14}N Corrole Nuclei

nucleus	$\lvert A_1\rvert$ (MHz)	$\lvert A_2\rvert$ (MHz)	$\lvert A_3\rvert$ (MHz)	$\lvert Q_1\rvert$ (MHz)	Q_2 (MHz)	Q_3 (MHz)
^{14}N[a]	1.9	2.1	1.8	0.95	−0.26	−0.69

[a] All four corrole nuclei were considered to be equivalent. The $\mathbf{A}_3$ and $\mathbf{Q}_3$ axes point along the $\mathbf{g}_3$ axis, and the $\mathbf{Q}_1$ axis lies in the corrole plane and at 90° to the Co−N bond direction.

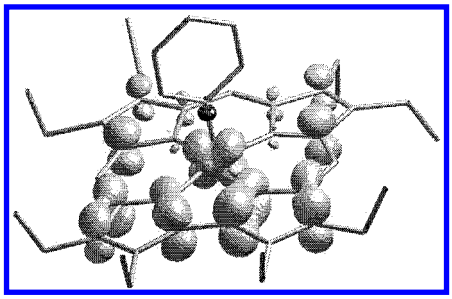

Figure 10. Spin density on the (OEC)Co(C_6H_5) complex determined by DFT calculations (level 0.0025).

Density Functional Computations

Density functional calculations provided a model for the spin density distribution in the complex (Figure 10), the SOMO of the cobalt ion and estimates for electronic couplings between the magnetic nuclei and the unpaired electron. We must emphasize that the precision of DFT calculations with present functionals is not overwhelming and quantitative agreement with the experimental data cannot be expected, but we do believe the results can be used with confidence in a qualitative discussion. An extensive comparison of DFT computations with different functionals and basis sets with detailed and well understood experimental results on cobaltous tetraphenylporphyrin(pyridine) and a series of related compounds, which supports this conviction, will be published elsewhere.[53]

DFT calculations put the unpaired electron in the d_{yz} molecular orbital of the cobalt ion, with the corrole coordinate system defined in Figure 1. The cobalt hyperfine matrix has principal values of $A_1 \sim -127$ MHz, $A_2 \sim 29$ MHz, and $A_3 \sim 40$ MHz which point in the *x*-, *y*-, and *z*-directions, respectively (Figure 1). As shown in Figure 10, the spin density determined by the DFT calculations conforms roughly to the C_{2v} pseudosymmetry of the macrocycle. Significantly more spin density is predicted on the bipyrrole unit (see also N_1 and N_4 in Figure 1) than on the other two pyrrole rings (see N_2 and N_3 in Figure 1). The aggregate spin density on the macrocycle is 65% with the remaining 35% being almost exclusively in the cobalt d_{yz} orbital.

The calculated **Q** tensors of the ^{2}H meso nuclei all have principal values of $Q_1 \sim -55$ kHz, $Q_2 \sim -45$ kHz, and $Q_3 \sim 100$ kHz, with the $\mathbf{Q}_3$ axis directed along the respective C−H bond. The ^{1}H hyperfine principal values of H_5 and H_{15} are similar, having $A_1 \sim -1.4$ MHz, $A_2 \sim -0.4$ MHz, and $A_3 \sim 1.6$ MHz with the $\mathbf{A}_3$ axis directed approximately toward N_1 and N_4, respectively, with the nitrogen nuclei on the side of the complex with the largest spin density. The **A** matrix of H_{10} is approximately coaxial to the **Q** tensor with values of $A_{1,2} \sim 0.8$ MHz and $A_3 \sim -0.6$ MHz. Due to the significant spin density on the macrocycle and its bias in favor of the bipyrrole unit, the proton hyperfine matrixes are not axial and none of the principal axis directions point at the cobalt ion.

Nitrogen N_1 and N_4 have significantly more p orbital spin density than N_2 and N_3, which is reflected by the hyperfine matrix, with $A_{1,2} \sim -2$ MHz, $A_3 \sim 7$ MHz for N_1 and N_4, and $A_{1,2} \sim -2$ MHz, $A_3 \sim -0.5$ MHz for N_2 and N_3. In fact, the computation predicts significantly different isotropic hyperfine couplings for N1 (∼1 MHz) and N4 (∼0.5 MHz). This deviation of the spin density from expectations based on the C_{2v} pseudosymmetry of the macrocycle is due to the orientation of the phenyl ligand which breaks this symmetry. In frozen solution, this orientation may well vary and the hyperfine couplings might thus be distributed. For all nitrogen nuclei the $\mathbf{A}_3$ axis points approximately along the normal to the corrole plane. The calculated **Q** tensors all have $e^2qQ/4h \sim 0.47$ MHz, but η varies between 0.04 and 0.83. The $\mathbf{Q}_1$ axis is directed normal to the respective Co−N bonds and is in the plane of the macrocycle.

The calculated ^{13}C phenyl hyperfine principal values of the directly coupled carbon with −9, −9 and −10 MHz are quasi-isotropic. The ortho, meta, and para carbons have principal values ranging from 1.3 to −1.0 MHz, −0.5 to −1.0 MHz, and −0.5 to 0.5 MHz, respectively.

Finally and significantly, DFT calculations predicted that ethyl protons have hyperfine couplings with principal values of up to 10 MHz. This outcome provides additional evidence that the largest couplings observed in the ^{1}H ENDOR spectra can indeed be assigned to the ethyl protons.

Discussion

Both our experimental and DFT data indicate a d^5 low-spin Co(IV) complex with the unpaired electron in the d_{yz} molecular orbital of the cobalt ion. Significant spin density was also measured and calculated to be on the macrocycle. Experimentally relatively small couplings from ^{14}N corrole nuclei, phenyl ^{13}C and ^{1}H nuclei, meso ^{1}H (^{2}H) nuclei, and ethyl ^{1}H nuclei could be observed. The magnitude of the ethyl ^{1}H hyperfine couplings is however too large to be explained by considering the electron to be 100% localized on the cobalt ion. Using the point dipole−dipole approximation and a cobalt-to-ethyl-proton distance of 0.53 nm, a maximum dipole contribution of only $2T = 1.1$ MHz is calculated, as compared to ∼5.7 MHz found experimentally. The experimental data can only be explained by assuming considerable spin density on the macrocycle. This conclusion is further supported by the DFT calculations (showing ethyl ^{1}H couplings up to 10 MHz) and the NMR measurements of Will et al.[7] who found large downfield shifts of the ethyl proton resonances. Additionally, having spin density on the macrocycle explains the noncoaxiality of the **g** and cobalt hyperfine matrixes principal directions, since the **g** principal directions will be influenced by spin−orbit coupling from both the macrocycle and the cobalt ion.

The DFT model provides a qualitative spin density model in general agreement with experimental data. The calculated and experimental values of the hyperfine and nuclear quadrupole interactions differ by up to a factor of 2. For example, the calculated $\mathbf{A}^{Co}$ principal values are approximately twice as large as those found experimentally but do have one large ($|A_1|$) and two small ($|A_2|$ and $|A_3|$) values, and the same orientation.

The experimentally determined nuclear quadrupole tensors of the three meso deuterons agree well with the DFT calculations both in magnitude and direction and are also similar to results found experimentally in related complexes.[48−50] By assuming the $\mathbf{Q}_1$ axes of the three nuclear quadrupole tensors point along the C−H bond directions, we were able to infer the orientation of the **g** matrix with respect to the molecular frame. The hyperfine matrixes of H_5 and H_{15} were found to be noncoaxial with the **Q** tensors and their main axes do not point at the cobalt ion. These results are also in qualitative agreement with the DFT calculations and provide further evidence supporting the conclusion that there is considerable spin density on the macrocycle.

The hyperfine matrixes and quadrupole tensors of the four corrole nitrogens could only be estimated and no discrimination between the four nuclei could be made, due to the low resolution of the frozen solution spectra and the complexity of a spin system with four $I = 1$ nuclei. ESEEM and HYSCORE spectra established that there are ^{14}N nuclei close to the "exact

cancellation" regime at X-band over the entire spectral range. Satisfactory simulation of the data was achieved assuming that the four ^{14}N corrole nuclei are equivalent. Simulations using the **A** matrixes and **Q** tensors from the DFT calculations, which gives a large difference between N_1,N_4 and N_2, N_3 (due to the large anisotropy in the spin density distribution) was found to be inconsistent with the experimental data. The X-band results therefore suggest that the anisotropy between the four nitrogens is overestimated by the DFT calculations. However, we cannot definitely exclude the possibility that some of the corrole nitrogens could have a very low modulation depth and were therefore not observed in the experiments. This situation appears to be unlike though, particularly as there was also no evidence from the ENDOR data. The experimental and DFT calculated nuclear quadrupole interactions are similar in magnitude but not in the η values (experimental $K = 0.475$ MHz, η=0.446 and calculated $K \sim 0.47$ MHz but η ranges from 0.04 to 0.83). The assignment of the $\mathbf{Q}_1$ axis as given in Table 4 (at 90° to the Co−N bond direction) is based on findings from CuTPP[54] and is consistent with the DFT calculations.

The DFT calculated hyperfine couplings for the directly coordinated phenyl ^{13}C nucleus (−9, −9 and −10 MHz) are overestimated by a factor of 2 in comparison to experimental values (|4.2|, |4.2|, and |4.0| MHz). However, both results have an anisotropy which is much smaller than if the spin density was considered to be 100% on the cobalt ion (the point-dipole model with a C−Co bond distance of 0.194 nm gives $2T = 5.4$ MHz at $g \sim 2.0$). The isotropic value observed experimentally can be explained by assuming a distribution of spin density on both the cobalt ion and the macrocycle.

From their data Will et al.[7] assigned the (OEC)Co(C_6H_5) complex as a resonance hybrid between a π cation radical and a Co(IV) complex,

$$(\mathrm{OEC})\mathrm{Co}^{\mathrm{IV}}(\mathrm{C_6H_5}) \leftrightarrow (\mathrm{OEC}^{\bullet+})\mathrm{Co}^{\mathrm{III}}(\mathrm{C_6H_5}) \qquad (5)$$

with the unpaired electron occupying the $d_{x^2-y^2}$ cobalt molecular orbital (see note 13 for corrole axes definition). It is instructive to compare our data to this model and also to data from known π cation radicals and metal centered complexes with corrole and porphyrin ligands.

A number of studies have investigated cobalt(III) tetraphenylporphyrin π cations generated by electrochemical oxidation. CW spectra in both solution and frozen solution typically show an isotropic g value of ∼2.00 and a width of $\Delta B \sim 5$ mT.[55,56] Sometimes nitrogen and cobalt hyperfine interactions are resolved.[44,57]

The electrochemistry of corroles with a variety of metal centers has been studied and examples of metal centered and macrocycle centered oxidations and reductions have been reported. Corrole cation radicals have been produced with the metal centers Co,[6] Sn,[10] Ni, and Cu.[12] The CW EPR spectra in frozen solution of these radical species are similar to the porphyrins with isotropic EPR spectra at $g \sim 2.00$ with a width of $\Delta B \sim 5$ mT (see Table 1). Metal centered oxidations and reductions have also been reported that generate low-spin d^5 complexes. The one-electron oxidation and reduction of (OEC)-$Fe^{IV}(C_6H_5)$ generates the d^5 low-spin Fe(III) complexes $[(\mathrm{OEC})\mathrm{Fe}^{\mathrm{III}}(\mathrm{C_6H_5})]^-$ and $[(\mathrm{OEC})\mathrm{Fe}(\mathrm{C_6H_5})]^+$ respectively, with g values of 2.51, 2.19, and 1.93, and 2.17, 2.04, and 2.01, respectively.[58] The spectrum of electrogenerated [(OMTPC)-$Co^{IV}(PPh_3)]^+$ [59] was also proposed to have a Co(IV) metal ion based on its EPR spectrum with g values of 2.14, 2.00, and 1.89. These three complexes have rhombic EPR spectra and g values that are very similar to those of $[(\mathrm{OEC})\mathrm{Co}^{\mathrm{IV}}(\mathrm{C_6H_5})]$. Several non-porphyrin complexes possessing a Co(IV) metal ion also have anisotropic EPR parameters comparable to those of $(\mathrm{OEC})\mathrm{Co}^{\mathrm{IV}}(\mathrm{C_6H_5})$.[60−63]

The CW EPR spectrum of (OEC)Co(C_6H_5) in toluene at room temperature consists of a single anisotropic line with a width of approximately 17 mT with no resolved hyperfine interactions. In a frozen toluene solution the spectrum is rhombic with partially resolved ^{59}Co hyperfine interactions. These data are most consistent with a complex where significant spin density is at the cobalt ion. The spin density on ^{59}Co is difficult to determine from its hyperfine matrix since the calculation involves contributions from electron density in the s and d orbitals which can have opposite signs.[64]

Constraints on the possible d orbital of the unpaired electron of the cobalt ion can be imposed by comparing couplings from the ^{14}N corrole nuclei and the directly coordinated ^{13}C phenyl nucleus with those from related and well characterized complexes. The d_{xy} configuration can be ruled out since this results in a strong overlap with the sp^2 hybrid orbitals of the corrole nitrogens and therefore in large ^{14}N couplings, examples being CuTPP and AgTPP where the ^{14}N hyperfine interactions are larger than 40 MHz.[54] These values are much larger than the ∼2 MHz of the^{14}N corrole nuclei in (OEC)Co(C_6H_5). Complexes where the unpaired electron mainly occupies a d_{z^2} orbital have large couplings with the axial ligands, examples being $(\mathrm{TPP})\mathrm{Co}^{\mathrm{II}}(\mathrm{P(Me)_3})$ where the ^{31}P coupling is ∼65 MHz[65] or $\mathrm{Co}^{\mathrm{II}}$TPP(py),[66] $\mathrm{Co}^{\mathrm{II}}$OEP(py),[67] and vitamin B_{12r}[68] where the isotropic hyperfine coupling with the directly coordinated axial ^{14}N nucleus is approximately $a_{iso} = 40$ MHz. This coupling is much larger than $a_{iso} \sim 4.1$ MHz observed for the directly coordinated phenyl ^{13}C nuclei in (OEC)Co(C_6H_5). Furthermore, five-coordinated complexes with a d_{z^2} configuration have strong solvent interactions[64] which can be observed with ENDOR or ESEEM. However, only a matrix line contribution from the solvent protons was observed for (OEC)Co(C_6H_5) in toluene, as revealed by ENDOR measurements. These simple arguments leave only the configuration $(d_{xz}d_{yz})^4(d_{x^2-y^2})^1$ or $(d_{x^2-y^2})^2(d_{xz}d_{yz})^3$ as possible candidates. On the bases of the experimentally determined $\mathbf{A}^{Co}$ matrix and DFT calculations, we propose that the cobalt ion contributes an orbital with d_{yz} character to the SOMO of the complex.

This conclusion is contrary to the $d_{x^2-y^2}$ orbital proposed by Will et al.,[7] which was based mainly on a comparison between g values of (OEC)Co(C_6H_5) and low-spin isoelectronic Fe(III) porphyrins with ground states ranging from $(d_{xz}d_{yz})^4(d_{x^2-y^2})^1$ to $(d_{x^2-y^2})^2(d_{xz}d_{yz})^3$.[13,69] For low-spin iron porphyrins the electronic configuration is often analyzed using the theory of Griffith[70] and Taylor[71] which considers only d_{xz}, d_{yz}, and $d_{x^2-y^2}$ orbitals to predict $\Sigma g_i = 12$ for $(d_{xz}d_{yz})^4(d_{x^2-y^2})^1$ and $\Sigma g_i = 16$ for $(d_{x^2-y^2})^2(d_{xz}d_{yz})^3$. The (OEC)Co($C_6H_5$) complex gives $\Sigma g_i = 12.4$, which leads Will et al. to suggest a $(d_{xz}d_{yz})^4(d_{x^2-y^2})^1$ configuration. However, we have shown that in (OEC)Co(C_6H_5) the orientation of the **g** matrix is determined by both spin density on the cobalt ion and on the macrocycle, which results in noncoaxial **g** and $\mathbf{A}^{Co}$ matrixes. This ligand−atom spin−orbit coupling rules out the use of the above theory from the onset. The fact that the g values of (OEC)Co(C_6H_5) are quite different from that predicted for a metal−ion centered complex with the unpaired electron in a d_{yz} orbital presumably indicates that the ligand−atom spin−orbit coupling is considerable.

A number of metal complexes with the unpaired electron in a d_{yz} orbital have been collected in Table 1. The five coordinated dithiolenes (e.g., $\mathrm{Co(S_2C_2(CF_3)_2)_2(P(OPh)_3)}$) were assigned to a d_{xz}/d_{yz} hybridized SOMO and have $g_{||} \sim 1.99$, $g_{\perp} \sim 2.03$, and

$A_{||}^{Co} \sim 183$ MHz, $A_{\perp}^{Co} \sim 21$ MHz.[59] The **g** and $\mathbf{A}^{Co}$ principal axes were found to be noncoaxial and dependent upon the degree of hybridization. However, in (OEC)Co(C_6H_5) we suggest that ligand-atom spin−orbit coupling causes the noncoaxiality of the **g** and $\mathbf{A}^{Co}$ principal axes.[72] The (OEC)Co(C_6H_5) complex has some features in common with several cobalt(II) complexes with Schiff bases and related ligands also possessing a $(d_{xy})^2$-$(d_{xz}d_{yz})^3$ ground state.[73,74] For example, the Co(II)CF_3(acacen) complex shown in Table 1 has a $\mathbf{A}^{Co}$ matrix with the largest principal value in the molecular plane of the molecule, and a large difference between the two *g* values in this plane (g_1 and g_2). The absolute values are not comparable however since this Co(II) complex has the electron localized on the metal ion. The oxygenated cobalt(II) complexes (oxyCo)TPP(py) and (oxyCo)-TPP(1-MeIm) have several key features in common with the (OEC)Co(C_6H_5) complex.[75] The unpaired electron spin density, although mainly on the O_2^- moiety, has a significant percentage located in the cobalt d_{yz} orbital. The $\mathbf{A}^{Co}$ matrix has essentially the same features as that of (OEC)Co(C_6H_5), with principal values $A_x = -53$ MHz and $A_{y,z} = -22$ MHz, and the $\mathbf{A}_x$ principal axis in the macrocycle plane.

Conclusion

A CW and pulse EPR and ENDOR study, combined with DFT calculations, allowed a detailed description of the electronic structure of (OEC)Co(C_6H_5). The principal *g* and cobalt hyperfine values were determined using CW EPR at both X- and Q-band. The principal **g** and $\mathbf{A}^{Co}$ axes directions with respect to the molecular frame are determined by CW EPR measurements on (OEC)Co(C_6H_5) aligned in a liquid crystal and by simulation of the ^{1}H and ^{2}H ENDOR spectra of the meso nuclei. By measuring and comparing Davies- and Mims-ENDOR spectra from (OEC)Co(C_6D_5), (OEC)Co($^{13}C_6H_5$), (D_3-OEC)-Co(C_6H_5), and (OEC)Co(C_6H_5) in toluene and d_8-toluene we were able to identify signals and determine magnetic interaction parameters from ^{1}H ethyl protons; ^{1}H, ^{2}H, and ^{13}C phenyl nuclei; and ^{1}H and ^{2}H meso nuclei. Magnetic interactions with the four nitrogen nuclei of the corrole ring produced deep modulations at X-band using three-pulse ESEEM and HYSCORE experiments.

Our data are consistent with a $S = {}^1/_2$ complex where the unpaired electron has spin density in the cobalt d_{yz} orbital (Co-(IV) character) and on the macrocycle (π cation radical character). This conclusion was formulated from (1) the ^{1}H ethyl proton hyperfine couplings, which were relatively large, and the hyperfine coupling of the directly coordinated ^{13}C phenyl nuclei which is isotropic. Interpretation of these two observations is afforded with a model where significant spin density is on the macrocycle, (2) the noncoaxiality between the **g** and $\mathbf{A}^{Co}$ principal axes, implying a spin−orbit interaction from the ligand nuclei, and (3) The NMR data from Will et al.,[7] which showed ethyl resonances that were significantly broadened and shifted downfield. DFT calculations are in good qualitative agreement with the experimental results.

Acknowledgment. We are grateful to the Swiss National Science Foundation for their support. Martin Bröring thanks the Deutsche Forschungsgemeinschaft for financing.

Supporting Information Available: Figures 1S: Matched Q-band HYSCORE spectra of (OEC)Co(C_6H_5). Figure 2S: X-band Davies-ENDOR spectra of (OEC)Co(C_6H_5). Figure 3S: Q-band Davies-ENDOR spectra of (OEC)Co(C_6H_5). Figure 4S: Q-band Mims-ENDOR spectra of (OEC)Co(C_6H_5). This material is available free of charge via the Internet at htpp://pubs.acs.org.

References and Notes

(1) Banerjee, R., Ed. *Chemistry and Biochemistry of B_{12}*; John Wiley & Sons: New York, 1999. [2080627.]

(2) *Vitamin B_{12} and B_{12}−Proteins. Lectures presented at the 4th European Symposium on Vitamin B12 and B12−Proteins*; Kräutler, B., Arigoni, D., Golding Weinheim, B. T., et al.; Ed.; Wiley-VCH: New York, 1998. [1735015.]

(3) Halpern, J. In *B12*; Wiley: New York, 1982, p 501 and references therein.

(4) Fukuzumi, S.; Miyamoto, K.; Suenobu, T.; Caemelbecke, E.; Kadish, K. M. *J. Am. Chem. Soc.* **1998**, *120*, 2880.

(5) Adamian, V. A.; D'Souza, F.; Licoccia, S.; Di Vona, M. L.; Tassoni, E.; Paolesse, R.; Boschi, T.; Kadish, K. M. *Inorg. Chem.* **1995**, *34*, 532.

(6) Kadish, K. M.; Adamian, V. A.; Van Caemelbecke, E.; Gueletii, E.; Will, S.; Erben, C.; Vogel, E. *J. Am. Chem. Soc.* **1998**, *120*, 11986.

(7) Will, S.; Lex, J.; Vogel, E.; Adamian, V. A.; Van Caemelbecke, E.; Kadish, K. M. *Inorg. Chem.* **1996**, *35*, 5577.

(8) Vogel, E.; Will, S.; Schulze Tilling, A.; Neumann, L.; Lex, J.; Bill, E.; Trautwein, A. X.; Wieghardt, K. *Angew. Chem., Int. Ed. Engl.* **1994**, *33*, 731.

(9) Van Caemelbecke, E.; Will, S.; Autret, M.; Adamian, V. A.; Lex, J.; Gisselbrecht, J. P.; Gross, M.; Vogel, E.; Kadish, K. M. *Inorg. Chem.* **1996**, *35*, 184.

(10) Kadish, K. M.; Will, S.; Adamian, V. A.; Walther, B.; Erben, C.; Ou, Z.; Guo N.; Vogel, E. *Inorg. Chem.* **1998**, *37*, 4573.

(11) Autret, M.; Will, S.; Van Caemelbecke, E.; Lex, J.; Gisselbrecht, J. P.; Gross, M.; Vogel, E.; Kadish, K. M. *J. Am. Chem. Soc.* **1994**, *116*, 9141.

(12) Will, S.; Lex, J.; Vogel, E.; Schmickler, H.; Gisselbrecht, J.-P.; Haubtmann, C.; Bernard, M.; Gross, M. *Angew. Chem., Int. Ed. Engl.* **1997**, *36*, 357; *Angew. Chem., Int. Ed. Engl.* **1997**, *109*, 367.

(13) We used the commonly adopted coordinate system for the corrole macrocycle with the *x*-axis chosen as a C_{2v} axis bisecting the N−Co−N angle as shown in Figure 1. This differs from the porphyrin macrocycle (D_{4h}) where the *x* and *y* axes point at the pyrrole nitrogens and are in the plane of the macrocycle. As a result the d_{xy} orbital in the "porphyrin" system becomes a $d_{x^2-y^2}$ orbital in the "corrole" system.

(14) Deligiannakis, Y.; Louloudi, M.; Hadjiliadis, N. *Coord. Chem. Rev.* **2001**, *204*, 1.

(15) Schweiger, A.; Jeschke, G. *Principles of Pulse Electron Paramagnetic Resonance*; Oxford University Press: Oxford, 2001.

(16) Gromov, I.; Shane, J.; Forrer, J.; Rakhmatoullin, R.; Rozentzwaig, Yu.; Schweiger, A. *J. Magn. Reson.* **2001**, *149*, 196.

(17) Schweiger, A. *Angew. Chem., Int. Ed. Engl.* **1991**, *30*, 265.

(18) Dikanov, S. A.; Tsvetkov, Y. D. *Electron Spin−Echo Modulation Spectroscopy*; CRC: Boca Raton, 1992.

(19) Höfer, P.; Grupp, A.; Nebenführ, H.; Mehring, M. *Chem. Phys. Lett.* **1986**, *132*, 279.

(20) Davies, E. R. *Phys. Lett.* **1974**, *A47*, 1.

(21) Mims, W. B. *Proc. R. Soc.* **1965**, *283*, 452.

(22) Gemperle, C.; Schweiger, A. *Chem. Rev.* **1991**, *91*, 1481.

(23) Wertz, J. E.; Bolton, J. R. *Electron Spin Resonance: Elementary Theory and Practical Applications*, 2nd ed.; Chapman and Hall: New York, 1986.

(24) Dikanov, S. A.; Xun, L.; Karpiel, A. B.; Tyryshkin, A. M.; Bowman, M. K. *J. Am. Chem. Soc.* **1996**, *118*, 8408.

(25) Astashkin, A. V.; Dikanov, S. A.; Tsvetkov, Yu, D. *J. Struct. Chem.* **1984**, *25*, 200.

(26) Flanagan, H. L.; Singel, D. J. *J. Chem. Phys.* **1987**, *87*, 5606.

(27) see web site: http://www.esr.ethz.ch.

(28) Smith, S. A.; Levante, T. O.; Meier, B. H.; Ernst, R. R. *J. Magn. Reson.* **1994**, *106*, 75.

(29) Madi, Z.; Van Doorslaer; S.; Schweiger; A. *J. Magn. Reson.* **2001**. Submitted for publication.

(30) Keijzers, C. P.; Reijerse, E. J.; Stam, P.; Dumont, M. F.; Gribnau, M. C. M. *J. Chem. Soc., Faraday Trans. 1* **1987**, *83*, 3493.

(31) Baerends, E. J.; Ellis, D. E.; Ros, P. *Chem. Phys.* **1973**, *2*, 41.

(32) Versluis, L.; Ziegler, T. *J. Chem. Phys.* **1988**, *322*, 88.

(33) te Velde, G.; Baerends, E. J. *J. Comput. Phys.* **1992**, *99*, 84.

(34) Fonseca Guerra, C.; Snijders, J. G.; te Velde, G.; Baerends, E. J. *Theor. Chem. Acc.* **1998**, *99*, 391.

(35) Frisch, M. J.; Trucks, G. W.; Schlegel, H. B.; Scuseria, G. E.; Robb, M. A.; Cheeseman, J. R.; Zakrzewski, V. G.; Montgomery, J. A., Jr.; Stratmann, R. E.; Burant, J. C.; Dapprich, S.; Millam, J. M.; Daniels, A. D.; Kudin, K. N.; Strain, M. C.; Farkas, O.; Tomasi, J.; Barone, V.; Cossi, M.; Cammi, R.; Mennucci, B.; Pomelli, C.; Adamo, C.; Clifford, S.; Ochterski, J.; Petersson, G. A.; Ayala, P. Y.; Cui, Q.; Morokuma, K.; Malick, D. K.; Rabuck, A. D.; Raghavachari, K.; Foresman, J. B.; Cioslowski, J.; Ortiz, J. V.; Stefanov, B. B.; Liu, G.; Liashenko, A.; Piskorz, P.; Komaromi,

I.; Gomperts, R.; Martin, R. L.; Fox, D. J.; Keith, T.; Al-Laham, M. A.; Peng, C. Y.; Nanayakkara, A.; Gonzalez, C.; Challacombe, M.; Gill, P. M. W.; Johnson, B. G.; Chen, W.; Wong, M. W.; Andres, J. L.; Head-Gordon, M.; Replogle, E. S.; Pople, J. A. *Gaussian 98*, revision A.7; Gaussian, Inc.: Pittsburgh, PA, 1998.

(36) *Titan 1.0*; Wavefunction, Inc. and Schrödinger, Inc.: Portland, Oregon, 1999. *Jaguar 3.5*; Schrödinger, Inc.: Portland, Oregon, 1998.

(37) Halgren, T. A. *J. Comput. Chem.* **1996**, *17*, 490; *J. Comput. Chem.* **1996**, *17*, 520; *J. Comput. Chem.* **1996**, *17*, 553.

(38) Halgren, T. A.; Nachbar, R. B. *J. Comput. Chem.* **1996**, *17*, 587.

(39) Halgren, T. A. *J. Comput. Chem.* **1996**, *17*, 616.

(40) van Lenthe, E.; Snijders, J. G.; Baerends, E. J. *J. Chem. Phys.* **1996**, *105*, 6505.

(41) Lide, D. R., Ed.; *Handbook of Chemistry and Physics*, 76th ed.; CRC Press: Boca Raton, 1995.

(42) Kay, C. W. M.; Di Valentin, M.; Möbius, K. *J. Chem. Soc., Perkin Trans.* **1997**, *2*, 2563.

(43) Neal, T. J.; Kang, S.-J.; Schulz, C. E.; Scheidt, W. R. *Inorg. Chem.* **1999**, *38*, 4294.

(44) Ichimori, K.; Ohya-Nishiguchi, H.; Hirota, N.; Yamamoto, K. *Bull. Chem. Soc. Jpn.* **1985**, *58*, 623.

(45) Schweiger, A.; Rudin, M.; Günthard, Hs. H. *Chem. Phys. Lett.* **1983**, *95*, 285.

(46) Michaeli, S.; Soffer, S.; Levanon, H.; Senge, M. O.; Kalisch, W. W. *J. Phys. Chem. A* **1999**, *103*, 1950.

(47) Rist, G.; Hyde, J. *J. Chem. Phys.* **1970**, *52*, 4633.

(48) Doan, P. E.; Fan, C.; Hoffman, B. M. *J. Am. Chem. Soc.* **1994**, *116*, 1033.

(49) Edmonds, D. T. *Phys. Rep.* **1974**, *A29*, 233

(50) *Landolt-Börnstein, Numerical Data and Functional Relationships in Science and Technology, Group III, volume 20, Nuclear Quadrupole Spectroscopy Data, Subvolume a*; Springer-Verlag: Berlin, 1988.

(51) DeRose, V. J.; Liu, K. E.; Lippard, S. J.; Hoffman, B. M. *J. Am. Chem Soc.* **1996**, *118*, 121.

(52) Ragle, J. L.; Mokarram, M.; Presz, D.; Minott, G. *J. Magn. Reson.* **1975**, *20*, 195.

(53) Jeschke, G.; Van Doorslaer, S., private communication.

(54) Brown, T. G.; Hoffman, B. M. *Mol. Phys.* **1980**, *39*, 1073.

(55) Kadish, K. M.; Lin, X. Q.; Han, B. C. *Inorg. Chem.* **1987**, *26*, 4161.

(56) Wolberg, A.; Manassen, J. *J. Am. Chem. Soc.* **1970**, *92*, 2982.

(57) Ohya-Nishiguchi, H.; Khono, M.; Yamamoto, K. *Bull. Chem. Soc. Jpn.* **1981**, *54*, 1923.

(58) Van Caemelbecke, E.; Will, S.; Autret, M.; Adamian, V. A.; Lex, J.; Gisselbrecht, J.; Gross, M.; Vogel, E.; Kadish, K. M. *Inorg. Chem.* **1996**, *35*, 184.

(59) Carpenter, G. B.; Clark, G. S.; Rieger, A. L.; Rieger, P. H.; Sweigart, D. A. *J. Chem. Soc., Dalton Trans.* **1994**, 2903.

(60) Topich, J.; Halpern, J. *Inorg. Chem.* **1979**, *18*, 1339.

(61) Vol'pin, M. E.; Levitin, I. Ya.; Sigan, A. L.; Nikitaev, A. T. *J. Organomet. Chem.* **1985**, *279*, 263.

(62) Anson, F.; Collins, J. T.; Coots, R. J.; Gipson, S. L.; Richmond, T. G. *J. Am. Chem. Soc.* **1984**, *106*, 5037.

(63) Collins, T. J.; Powell, R. D.; Slebodnick, C.; Uffelman, E. S. *J. Am. Chem. Soc.* **1991**, *113*, 8419.

(64) Van Doorslaer, S.; Schweiger, A. *Phys. Chem. Chem. Phys.* **2001**, *3*, 159.

(65) Wayland, B. B.; Abd-Elmageed, M. E. *J. Am. Chem. Soc.* **1974**, *96*, 4809.

(66) Van Doorslaer, S.; Bachmann, R.; Schweiger, A. *J. Phys. Chem. A* **1999**, *103*, 5446.

(67) Baumgarten, M. EPR und ENDOR Untersuchungen in Übergangsmetallkomplexen mit organischen Chelatliganden−Modellsysteme für katalytische und biologische Prozesse. Ph.D. Thesis, Free University of Berlin, Berlin, 1988.

(68) Jörin, E.; Schweiger, A.; Günthard Hs. H. *J. Am. Chem. Soc.* **1983**, *105*, 4227.

(69) Walker, F. A. in *The Porphyrin Hand Book*; Academic Press: London, 2000; Vol. 5, p 81.

(70) Griffith, J. S. *Proc. R. Soc. London, A* **1956**, *235*, 23.

(71) Taylor, C. P. S. *Biochim. Biophys. Acta* **1977**, *491*, 137.

(72) Stone, A. J. *Proc. R. Soc. London, Ser. A* **1963**, *271*, 424.

(73) Rudin, M.; Schweiger, A.; Berchten, N.; Günthard, Hs. H. *Mol. Phys.* **1980**, *41*, 1317.

(74) Daul, C.; Schläpfer, C. W.; von Zelewsky, A. *Structure and Bonding*; Springer-Verlag: Berlin, 1979; and references therein.

(75) Van Doorslaer, S.; Schweiger, A. *J. Phys. Chem. B* **2000**, *104*, 2919.